universe

IMPACT FACTOR 2.5

CITESCORE 4.3

Article

On Dark Matter and Dark Energy in CCC+TL Cosmology

Rajendra P. Gupta

Special Issue
Dark Energy and Dark Matter

Edited by
Prof. Dr. Yan Gong

MDPI

https://doi.org/10.3390/universe10060266

universe

MDPI

Article

On Dark Matter and Dark Energy in CCC+TL Cosmology

Rajendra P. Gupta

Department of Physics, University of Ottawa, Ottawa, ON K1N 6N5, Canada; rgupta4@uottawa.ca

Abstract: Relaxing the temporal constancy constraint on coupling constants in an expanding universe results in Friedmann equations containing terms that may be interpreted as dark energy and dark matter. When tired light (TL) was considered to complement the redshift due to the expanding universe, the resulting covarying coupling constants (CCC+TL) model not only fit the Type Ia supernovae data as precisely as the ΛCDM model, but also resolved concerns about the angular size of cosmic dawn galaxies observed by the James Webb Space Telescope. The model was recently shown to be compliant with the baryon acoustic oscillation features in the galaxy distribution and the cosmic microwave background (CMB). This paper demonstrates that dark energy and dark matter of the standard ΛCDM model are not arbitrary but can be derived from the CCC approach based on Dirac's 1937 hypothesis. The energy densities associated with dark matter and dark energy turn out to be about the same in the ΛCDM and the CCC+TL models. However, the critical density in the new model can only account for the baryonic matter in the universe, raising concerns about how to account for observations requiring dark matter. We therefore analyze some key parameters of structure formation and show how they are affected in the absence of dark matter in the CCC+TL scenario. It requires reconsidering alternatives to dark matter to explain observations on gravitationally bound structures. Incidentally, since the CCC models inherently have no dark energy, it has no coincidence problem. The model's consistency with the CMB power spectrum, BBN element abundances, and other critical observations is yet to be established.

Keywords: cosmology; galaxies; early universe; high-redshift; dark matter; dark energy; cosmic dawn

Citation: Gupta, R.P. On Dark Matter and Dark Energy in CCC+TL Cosmology. *Universe* **2024**, *10*, 266. https://doi.org/10.3390/universe10060266

Academic Editor: Yan Gong

Received: 14 May 2024
Revised: 14 June 2024
Accepted: 14 June 2024
Published: 18 June 2024

1. Introduction

Dark matter and dark energy are considered the pillars of modern cosmology, defined by the cold dark matter and cosmological constant Λ that Einstein had introduced in his general theory of relativity for establishing the steady state universe. He later rejected Λ. However, the constant was resurrected by cosmologists to explain the universe's accelerated expansion confirmed by Type 1a supernovae (SNe1a) observations [1,2] after the launch of the Hubble telescope. Most studies have endorsed the accelerating expansion of the universe e.g., [3–6]. Putting Λ back into the Einstein equations resulted in the simplest form of Friedmann equations that could explain the increasingly higher redshift versus luminosity relation of SNe1a and other astrophysical and cosmological observations better than any alternatives. It resulted in an energy density in the universe with constant value and negative pressure corresponding to Λ, and a matter energy density that is six times what can be accounted for by the baryonic matter we all are familiar with. The former is dubbed dark energy and the unaccounted matter as dark matter because the origin of either of them is not yet understood and is not directly verifiable. Extensive effort in cosmology and particle physics is being devoted to proving the existence of these elusive dark entities without any sign of their direct detection.

Indirect proof of the existence of dark matter is plentiful (see Bahcall [7] for a succinct review) albeit with inconsistencies e.g., [8,9], including the too-big-to-fail problem e.g., [10], the cusp-core problem [11–13], and the missing satellite problem [14]. Lord Kelvin in 1884 [15] derived the number of dark bodies by analyzing the velocity dispersion of the

stars orbiting the center of the Milky Way and concluded, "Many of our supposed thousand million stars, perhaps a great majority of them, maybe dark bodies." The flat rotation curves of spiral galaxies that initially suggested the possibility of dark matter [16] and provided a solid basis for the existence of dark matter [17–21] are for nearby (local) galaxies, and not universal. This limitation was due to the difficulty of observing rotation velocities in distant galaxies. With improved instrumentation and accumulating data for a stack of galaxies, Genzel et al. [22] and Lang et al. [23] have recently determined galaxy rotation curves for a stack of ∼100 galaxies at $0.6 < z < 2.6$; i.e., more distant than 5 billion light years, and established the common rotation curve that falls off rapidly with radius (Figure 2b of [22]), unlike the rotation curves of nearby galaxies (Figure 3 of [18]). Quoting Nelson and Williams [24] in the context of non-local galaxies, "Only a simulation without a dark matter halo is able to reproduce the observed rotation curves." They also state the following: "So if it turns out that the rotation curves for all distant galaxies are steeply falling, then this implies that galaxies form initially without a massive dark matter halo. But this is contrary to the accepted paradigm for galaxy formation, where the dark matter halo collapses first, followed by the infall of the baryonic matter into the gravitational potential well of the dark matter, where it forms visible stars."

Other methods of indirectly observing dark matter include (a) stellar velocity dispersion in globular clusters and galaxies e.g., [25,26], (b) mass estimate of galaxy clusters by three methods e.g., [27]—virial mass, gravitational lensing, and hydrostatic equilibrium of the intracluster medium, (c) gravitational lensing e.g., [28,29]; (d) cosmic microwave background (CMB) temperature anisotropy [30,31], (e) structure formation e.g., [32–34], (f) bullet cluster e.g., [35], (g) baryon acoustic oscillation (BAO) features in galaxy distribution e.g., [36,37], and (h) SNe1a [38,39].

Inconsistencies in determining the contents of dark matter in different observations have been a subject of debate about the very existence of dark matter e.g., [22–24,40,41]. Its unambiguous and conclusive direct detection continues to be elusive. The primary purpose of the European Space Agency's Euclid satellite, launched on 1 July 2023, is to map the geometry of the universe through the distribution of galaxies to know about the dark sector—the invisible dark energy and dark matter [42]. Several experiments of direct detection of dark matter particles have been planned worldwide, such as deep underground experiments in facilities similar to those used for neutrino detection e.g., [43] and using the Large Hadron Collider (LHC) to detect dark matter particles produced in collisions of the LHC proton beams e.g., [44,45].

Several alternatives to dark matter and dark energy theories have been proposed. Mannheim [46] reviewed them generically as follows: "that it is a universal acceleration scale which determines when a luminous Newtonian expectation is to fail to fit data, that there is a global cosmological effect on local galactic motions which can replace galactic dark matter, and that to solve the cosmological constant problem it is not necessary to quench the cosmological constant itself, but only the amount by which it gravitates". Milgrom in1983 [47] proposed the modification of Newtonian dynamics (MOND) in very small acceleration domains to account for the flat rotation curves in then observable galaxies (see also [48–51]). Recently, he has interpreted MOND as a theory of modified inertia [52]. MOND can be considered as a modified gravitational theory. Other such theories replacing dark matter and dark energy include the relativistic generalization of MOND in the form of tensor-vector-scalar gravity (TeVeS) [53], f(R) gravity [54], negative mass, dark fluid [55], entropic gravity [56], dark dimension e.g., [57], retarded gravity e.g., [58–60], and others e.g., [46,61]. We do not intend to review the extensive literature about the application of MOND, its relativistic adaptation, and other alternatives that refute the existence of dark matter and dark energy; we have just cited typical references. One strong criticism of such theories has been that they are not compliant with the CMB anisotropy and matter power spectra observations, but Skordis and Złośnik [62] have put such criticism to rest.

The most accepted model based on Einstein's cosmological constant Λ and the cold dark matter, known by the acronym ΛCDM, is relatively simple to use in diverse applica-

tions, but not always compliant with observations. Chief noncompliance with the model was noticed in the cosmic dawn observations by the James Webb Space Telescope (JWST) in the formation of nascent stars and galaxies and the creation of the reionization era. The galaxies were more massive and evolved, higher in number, and smaller in physical size than predicted e.g., [63–80]. While most astronomers scurried to revise their galaxy formation model to fit the observations within the ΛCDM cosmology by compressing the timeline for the formation of Population III stars and galaxies, such as by considering the presence of primordial massive black hole seeds and super Eddington accretion rates in the early universe e.g., [70,81–97], others saw the potential of going beyond the ΛCDM cosmology [12,98–106]. One such effort [39] used the evolving coupling constants, inspired by Dirac's hypothesis [107], and the tired light phenomenology of Zwicky [108] for explaining observed redshift, to develop a new model that could naturally explain the JWST observations with the parameters obtained by fitting the SNe1a Pantheon+ data [109,110]. The new model exploits the interrelationship in the variation of various coupling constants [111] and the assumption that the redshifts due to the expanding universe and the tired light occur concurrently. Since the light travels the same proper distance for the two redshifts, the new model has no more free parameters than the ΛCDM model. The hybrid model was christened CCC+TL, CCC for covarying coupling constants (not to be confused with Penrose's Conformal Cyclic Cosmology), and TL for the tired light. More recently, this model was shown to fit the position of the baryon acoustic oscillation (BAO) feature observed in the large-scale distribution of galaxies and the angular size of the sound horizon due to BAO imprinted in the cosmic microwave background (CMB) anisotropy [37]. This model has no dark matter or dark energy per se, but its compact equations can be expanded to relate to the dark matter and dark energy in the ΛCDM model.

While the paper [39] does not discuss dark matter and dark energy aspects of the new model, the paper [37] discusses it only subtly. The current paper attempts to show how parameter α in the new models can be explicitly interpreted as dark matter and dark energy in the ΛCDM model. It attempts to show that the absence of dark matter does not negatively affect the formation of galaxies primarily due to the increased age of the universe. Additionally, it shows that due to the tired light contribution to the redshift being rather small, the model is consistent with the time dilation data. Essentially, the current paper aims to show the similarities and differences between the two models with respect to dark matter and dark energy, and analyze some key parameters of structure formation to understand how they are affected in the absence of dark matter in the CCC+TL model. Section 2 prepares the theoretical background. Section 3 presents estimates of dark matter and dark energy estimates. Section 4 deals with the galaxy formation concerns without dark matter. We discuss our findings in Section 5 and present conclusions in Section 6.

2. Theoretical Background

In cosmology, the scale factor $a(t)$ accounts for the expansion of the universe. We introduced another scale factor, $f(t)$, to consider the possibility of the length dimension of constants and the length unit evolving with the expansion. Then, the speed of light evolves as $c(t)\sim f(t)$, gravitational constant as $G(t)\sim f(t)^3$, Planck constant as $h(t)\sim f(t)^2$, and Boltzmann constant as $k(t)\sim f(t)^2$, i.e., $G\sim c^3\sim h^{3/2}\sim k^{3/2}$. This relationship can also be shown by the local energy conservation law [111]. It modifies the FLRW metric and thus the Einstein equations, resulting in Friedmann equations slightly different from their familiar form. The modified FLRW metric, incorporating the covarying coupling constant (CCC) concept in [39] is

$$\begin{aligned} ds^2 = \; & c_0^2 dt^2 f(t)^2 - a(t)^2 f(t)^2 \\ & \times \left(\tfrac{dr^2}{1-kr^2} + r^2 \left(d\theta^2 + \sin^2\theta d\phi^2 \right) \right), \end{aligned} \tag{1}$$

the modified Friedmann equations are

$$\left(\frac{\dot{a}}{a}+\alpha\right)^2=\frac{8\pi G_0}{3c_0^2}\varepsilon-\frac{\kappa c_0^2}{a^2}, \text{ and} \tag{2}$$

$$\frac{\ddot{a}}{a}=-\frac{4\pi G_0}{3c_0^2}(\varepsilon+3p)-\alpha\left(\frac{\dot{a}}{a}\right), \tag{3}$$

and the modified continuity equation is

$$\dot{\varepsilon}+3\frac{\dot{a}}{a}(\varepsilon+p)=-\alpha(\varepsilon+3p). \tag{4}$$

Here, G_0 is the current value of the gravitational constant, c_0 is the current value of the speed of light, κ is the curvature constant, α is a constant defining the variation of the constants through function $f(t)=\exp(\alpha(t-t_0))$ with the cosmic time t measured from the beginning of the universe and t_0 as the current time, ε is the energy density of all the components, and p is their pressure (It should be mentioned that the metric, Equation (1), can be transformed into the standard FLRW metric by redefining $t\rightarrow t'=(1/\alpha)\exp[\alpha(t-t_0)]$ and a new scale factor $a'(t)=a(t)f(t)$, thus yielding the standard Einstein tensor. However, when we write the complete Einstein equations [39], we find that we cannot eliminate $f(t)$ from the right-hand side; i.e., the right-hand side cannot be transformed into the standard form). Using the function $f(t)$, $c(t)=c_0f(t)$ and $G=G_0f(t)^3$ in the CCC model. The solution of Equation (4) for matter ($p=0$) and radiation ($p=\varepsilon/3$) are, respectively,

$$\varepsilon_m=\varepsilon_{m,0}a^{-3}f^{-1}, \text{ and } \varepsilon_r=\varepsilon_{r,0}a^{-4}f^{-2}. \tag{5}$$

Defining the Hubble expansion parameter as $H\equiv\dot{a}/a$, we may write Equation (2) for a flat universe ($\kappa=0$) as

$$(H+\alpha)^2=\frac{8\pi G_0}{3c_0^2}\varepsilon\Rightarrow\varepsilon_{c,0}^C\equiv\frac{3c_0^2(H_0+\alpha)^2}{8\pi G_0}. \tag{6}$$

This equation defines the current critical density $\varepsilon_{c,0}^C$ of the universe in the CCC model that depends not only on the Hubble constant but also on the constant α. Using Equations (5) and (6), we may write

$$(H+\alpha)^2=(H_0+\alpha)^2\left(\Omega_{m,0}a^{-3}f^{-1}+\Omega_{\mathrm{r},0}a^{-4}f^{-2}\right). \tag{7}$$

In this equation, relative matter density $\Omega_{m,0}\equiv\varepsilon_{m,0}/\varepsilon_{c,0}^C$ and relative radiation density $\Omega_{\mathrm{r},0}\equiv\varepsilon_{r,0}/\varepsilon_{c,0}^C$. Since $\Omega_{\mathrm{r},0}\ll\Omega_{\mathrm{m},0}$, and since we do not have to worry about the dark energy density in the CCC model, Equation (7) simplifies to the following [37]:

$$(H+\alpha)^2=(H_0+\alpha)^2\left(a^{-3}f^{-1}+\Omega_{\mathrm{r},0}a^{-4}f^{-2}\right). \tag{8}$$

However, we may expand and rewrite Equation (2) as

$$\begin{aligned}H^2&=\tfrac{8\pi G_0}{3c_0^2}\varepsilon-\alpha^2-2\alpha H\\&=\tfrac{8\pi G_0}{3c_0^2}\varepsilon-\alpha^2-2\alpha\left(\left(\tfrac{8\pi G_0}{3c_0^2}\varepsilon\right)^{1/2}-\alpha\right), \text{ or}\end{aligned}$$

$$H^2=\frac{8\pi G_0}{3c_0^2}\varepsilon+\alpha^2-2\alpha\left(\frac{8\pi G_0}{3c_0^2}\varepsilon\right)^{1/2}=\frac{8\pi G_0}{3c_0^2}\left(\varepsilon+\frac{3c_0^2}{8\pi G_0}\alpha^2-2\alpha\left(\frac{3c_0^2}{8\pi G_0}\right)^{-1/2}\varepsilon^{1/2}\right)\equiv\frac{8\pi G_0}{3c_0^2}(\varepsilon+\varepsilon_{de}+\varepsilon_u). \tag{9}$$

Here, ε is the composite energy density of matter and radiation, ε_{de} is the dark energy density, and ε_u is the unspecified (or unknown) energy density. In terms of the standard definition of the critical density $\varepsilon^S_{c,0} \equiv 3c_0^2H_0^2/8\pi G_0$, Equation (9) becomes

$$H^2 = H_0^2(\Omega_{m,0}a^{-3}f^{-1} + \Omega_{r,0}a^{-4}f^{-2} + \Omega_{de} + \Omega_{u,0}a^{-3/2}f^{-1/2}\Big).$$

Comparing with similar expressions for the ΛCDM model in a flat universe,

$$H^2 = \frac{8\pi G_0}{3c_0^2}\varepsilon + \frac{\Lambda}{3} = \frac{8\pi G_0}{3c_0^2}\left(\varepsilon + \frac{c_0^2}{8\pi G_0}\Lambda\right) \equiv \frac{8\pi G_0}{3c_0^2}(\varepsilon + \varepsilon_\Lambda), \text{ or}$$

$$H^2 = H_0^2(\Omega_{m,0}a^{-3} + \Omega_{r,0}a^{-4} + \Omega_\Lambda\Big), \tag{10}$$

We see that the cosmological constant term $\Lambda/3$ of the ΛCDM model is replaced by the constant α^2 in the CCC model. Additionally, there is an evolutionary term $2\alpha\left(8\pi G_0\varepsilon/3c_0^2\right)^{1/2}$. This term may be considered a dynamic component of the quintessence (time-varying) dark energy, as dark matter that evolves differently than the baryonic matter, or something yet unspecified or unknown (say U). Since α turns out to be negative, the contribution of U is positive.

Using Equation (6), Equation (9) may be written as

$$H^2 = (H + \alpha)^2 + \alpha^2 - 2\alpha(H + \alpha). \tag{11}$$

This equation can be written directly from Equation (2), but one may have difficulty seeing how it relates to the dark energy of the ΛCDM model. When divided by H_0^2, the equation at the current time becomes

$$1 = \frac{(H_0 + \alpha)^2}{H_0^2} + \frac{\alpha^2}{H_0^2} - \frac{2\alpha(H_0 + \alpha)}{H_0^2} \equiv \Omega_{m,0} + \Omega_{de} + \Omega_{u,0}. \tag{12}$$

Equivalently, for the ΛCDM model, Equation (10) results in

$$1 = \frac{8\pi G_0}{3c_0^2H_0^2}(\varepsilon_{m,0} + \varepsilon_\Lambda) \equiv \Omega_{m,0} + \Omega_\Lambda. \tag{13}$$

The critical density here is defined as $3c_0^2H_0^2/8\pi G_0$.

Permitting the tired light effect to coexist with the expanding universe splits redshift z into z_t and z_x, such that $(1 + z) = (1 + z_t)(1 + z_x)$, and the Hubble constant H_0 into H_t and H_x, such that $H_0 = H_t + H_x$; the subscript t is for tired light, and x is for expanding universe. It is done by equating the proper distances determined using the tired light effect and the expanding universe (see [39], Equations (34)–(47)). As a result, it does not involve any additional free parameters. However, it reduces the time dilation since tired light does not cause time dilation. We will take up this concern in Section 5—Discussion.

It should be emphasized that the function $f(t)$ evolves in an expanding universe, similar to the gravitational constant G evolving in Dirac's large number hypothesis due to the expansion of the universe [107]. Function $f(t)$ does not evolve in the tired-light-only universe (TL model).

One may be concerned about the covariance of the proposed model and related gauge issue. From a general perspective, a model that uses a Lagrangian with a function that is dependent on a particular coordinate breaks the covariance of the model theory. However, we could replace the function $f(t)$ by $f(x)$ in the Lagrangian, where x are the four spacetime coordinates. We will thus obtain covariant equations. Then, when we want to analyze a particular case, we can choose $f(x)$ in such a way that it depends only on t,

i.e., $f(x) \rightarrow f(t)$. This is the case when we have homogeneity and isotropy of the space section of the spacetime (typical of cosmological models). This is the approach that is used in several scalar-tensor models. Thus, the gauge issue does not arise when dealing with perturbations.

3. Dark Matter and Dark Energy Estimates

CCC Model: Referring to Table 1 in [39] and ignoring the uncertainties, we have for the ΛCDM model, $H_0 = 73.0$ Km s^{-1} Mpc^{-1} and $\Omega_{m,0} = 0.35$, whereas for the CCC model, $H_0 = 72.7$ Km s^{-1} Mpc^{-1} and $\alpha = -0.50H_0$. The critical density as defined by Equation (6) $\varepsilon^C_{c,0} \equiv 3c_0^2(H_0+\alpha)^2/8\pi G_0$, in terms of its standard definition $\varepsilon^S_{c,0} \equiv 3c_0^2H_0^2/8\pi G_0$, is then $(H_0+\alpha)^2/H_0^2 = 0.25$. It only comprises the matter density and the radiation density. However, if we use the expanded version given by Equation (12), we obtain $\Omega_{m,0} = 0.25$, $\Omega_{de} = 0.25$, and $\Omega_{u,0} = 0.50$ for the CCC model.

CCC+TL Model: For the CCC+TL model, obtained by combining the CCC expanding universe model with the tired light effect [39], the same table shows $H_0 = 72.6$ Km s^{-1} Mpc^{-1}, $H_x = 59.5$ Km s^{-1} Mpc^{-1}, and $\alpha = -0.80H_x$. The critical density, as defined by Equation (6), in terms of $3c_0^2H_x^2/8\pi G_0$, is then $(H_x+\alpha)^2/H_x^2 = 0.04$. However, $3c_0^2H_x^2/8\pi G_0$ is not the standard critical density $\varepsilon^S_{c,0} \equiv 3c_0^2H_0^2/8\pi G_0$; it is smaller by a factor of $H_x^2/H_0^2 = 0.67$. This means that the critical density for the CCC+TL model $\varepsilon^{CCC+TL}_{c,0} = 0.03\varepsilon^{\mathrm{S}}_{c,0}$, i.e., $\Omega_{m,0}$ today is 0.03 of the standard critical density, which is about the same as the baryon density of the standard model; $\Omega_{m,0}$ has no room for dark matter in the CCC+TL model; i.e., $\Omega_{m,0} \rightarrow \Omega_{b,0}$. Again, the critical density only comprises the matter density and the radiation density (insignificant at the current epoch and thus neglected), nothing else.

Let us now consider the expanded version of the CCC+TL model. In this case, tired light redshift does not contribute to the expansion of the universe. H_0 in Equation (12) must be replaced by H_x in the table; i.e., Equation (12) is modified as

$$1 = \frac{(H_x+\alpha)^2}{H_x^2} + \frac{\alpha^2}{H_x^2} - \frac{2\alpha(H_x+\alpha)}{H_x^2} \equiv \Omega_{m,0} + \Omega_{de} + \Omega_{u,0}. \tag{14}$$

We now obtain $\Omega_{m,0} = 0.04$, $\Omega_{de} = 0.64$, and $\Omega_{u,0} = 0.32$. We may thus relate Ω_{de} with the dark energy density Ω_Λ of the ΛCDM model, and $\Omega_{u,0}$ with something related to dark matter.

While we can relate the CCC's constant α with the dark energy of the ΛCDM model, there is no need to do so. *Accelerated expansion of the universe is caused by the weakening strength of the coupling constants* as proposed by Dirac [107], which in turn is caused by the evolving length dimension in the constants [111].

Matter-Radiation Equality: Next, we should determine at what values of redshift we have the dominance of radiation. From Equation (7), the matter-radiation equality in the new models occurs when

$$\Omega_{m,0}a^{-3}f^{-1} = \Omega_{\mathrm{r},0}a^{-4}f^{-2} \Rightarrow af = \Omega_{\mathrm{r},0}/\Omega_{m,0}. \tag{15}$$

Let us first consider the base CCC model for which the critical density is about 25% of its value for the standard model and $\Omega_{m,0} \cong 1$. Thus, the radiation density $\Omega^{\Lambda\mathrm{CDM}}_{r,0} \sim 9 \times 10^{-5}$ estimated for the ΛCDM model [112] increases by a factor of 4 to $\Omega^{\mathrm{CCC}}_{r,0} \sim 3.6 \times 10^{-4}$; matter-radiation equality happens at $af = (1+z)^{-1}f(z) = 3.6 \times 10^{-4}$. Since $f(z \gg 0) = 1.66$, we obtain $z_{rm} = 4610 \sim 4600$. In the expanded CCC model, the critical density is the same as in the standard model, but $\Omega_{m,0} = 0.25$. Therefore, $\Omega_{\mathrm{r},0}/\Omega_{m,0} = 3.6 \times 10^{-4}$, and redshift for the matter-radiation equality is again $z_{rm} = 4610 \sim 4600$.

Now, we consider the base CCC+TL model. We have determined above that $\varepsilon^{CCC+TL}_{c,0} = 0.03\varepsilon^{\mathrm{S}}_{c,0}$. Therefore, $\Omega^{CCC+TL}_{r,0} \sim 3 \times 10^{-3}$. Since $\Omega_{m,0} \cong 1$, we have $a_x f = (1+z_x)^{-1}f(z_x) = 3 \times 10^{-3}$, and since $f(z \gg 0) = 3.66$, $z_x = 1216$. Since $1+z = (1+z_x)(1+z_t)$, we need

to know z_t (the tired light component of the redshift) in order to obtain z_{rm}. We can easily obtain $z_t \approx 7$ (as per [39]), resulting in $z_{rm} = 9737 \sim 10,000$. For the expanded CCC+TL model, the critical density $\varepsilon_{c,0}^{CCC+TL} = 0.03\varepsilon_{c,0}^{S}$. However, the ratio $\Omega_{r,0}/\Omega_{m,0}$ does not change, and $z_{rm} \sim 10,000$.

For the ΛCDM model, the radiation matter equality occurs at $a = \Omega_{r,0}/\Omega_{m,0} = 9 \times 10^{-5}/0.35 = 2.6 \times 10^{-4}$, i.e., $z = 3888 \sim 4000$.

Matter-U Equality: This equality is meaningful only in the expanded CCC and CCC+TL models because the U energy density does not exist in the base models. It happens when

$$\Omega_{m,0} a^{-3} f^{-1} = \Omega_{u,0} a^{-3/2} f^{-1/2}. \tag{16}$$

For the expanded CCC model, as determined above, $\Omega_{m,0} = 0.25$ and $\Omega_{u,0} = 0.50$. It leads to $a^{-3/2} f^{-1/2} = 2$. It yields $z = 0.72$ with the numbers behind Figure 1 drawn using the equations from Gupta (2023). The U energy density is dominant at $z < 0.72$.

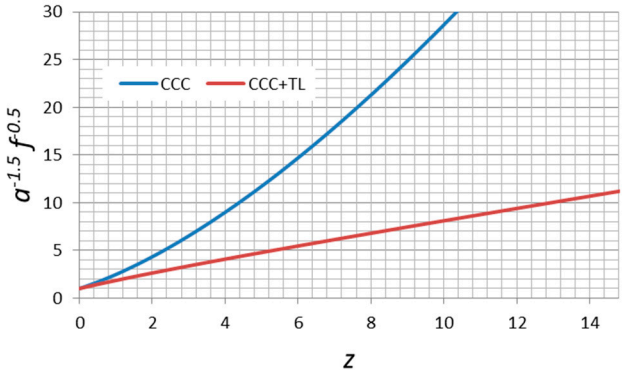

Figure 1. Variation of $a^{-3/2} f^{-1/2}$ with measured redshift z.

For the expanded CCC+TL, $\Omega_{m,0} = 0.04$ and $\Omega_{u,0} = 0.32$. It leads to $a^{-3/2} f^{-1/2} = 8$. We now obtain $z = 10$ using the numbers behind Figure 1, meaning that U energy density is dominant at $z < 10$.

U-Dark Energy Equality: Again, this equality is meaningful only in the expanded CCC and CCC+TL models because the U and dark energy densities do not exist in the base models. The equality occurs when

$$\Omega_{u,0} a^{-3/2} f^{-1/2} = \Omega_{de}. \tag{17}$$

For the expanded CCC model, $\Omega_{de} = 0.25$, and $\Omega_{u,0} = 0.50$. Therefore, $a^{-3/2} f^{-1/2} = 0.5$. From Figure 1, it will happen in the future.

Considering now the expanded CCC+TL model, $\Omega_{de} = 0.64$ and $\Omega_{u,0} = 0.32$, giving $a^{-3/2} f^{-1/2} = 2$. It yields $z = 1.2$, meaning that the dark energy density is dominant at $z < 1.2$; i.e., at present, the same as for the ΛCDM model.

Matter-Dark Energy Equality for theΛCDM model: This happens when $\Omega_{m,0} a^{-3} = \Omega_\Lambda$, i.e., $a = (\Omega_{m,0}/\Omega_\Lambda)^{1/3} = 0.81$, i.e., $z = 0.23$. It is 0.29 using Planck collaboration [38] values of $\Omega_{m,0} = 0.3158$ and $\Omega_\Lambda = 0.6842$.

Accelerated Expansion: We can determine the redshift when the deceleration of the universe changes to acceleration from the second Friedmann equation (Equation (3)). Using Equations (2), (5) and (6) and $\Omega_{m,0} = 1$, since $\Omega_{r,0} \ll \Omega_{m,0}$,

$$\begin{aligned} \frac{\ddot{a}}{a} &= -\frac{4\pi G_0}{3c_0^2}(\varepsilon + 3p) - \alpha\left(\frac{\dot{a}}{a}\right) \\ &= -\frac{1}{2} a^{-3} f^{-1} - \frac{\alpha}{H_0 + \alpha} a^{-3/2} f^{-1/2} + \frac{\alpha^2}{(H_0+\alpha)^2} = 0. \end{aligned} \tag{18}$$

Defining $y \equiv a^{-3/2} f^{-1/2}$, we may write this equation as a quadratic equation:

$$\frac{1}{2}y^2 + \frac{\alpha}{H_0 + \alpha}y - \frac{\alpha^2}{(H_0 + \alpha)^2} = 0. \tag{19}$$

For the CCC model, $\alpha = -0.50H_0$, and the above equation becomes $y^2 - 2y - 2 = 0$, with the acceptable solution $y = 2.73$. This corresponds to $z = 1.15$. In this model, the universe has been accelerating since it was at the redshift of 1.15.

Giving consideration to the CCC+TL model, we have $\alpha = -0.80H_0$; recall that H_0 is really H_x in this case. Equation (19) now reduces to $y^2 - 8y - 32 = 0$, and its solution is $y = 10.9$, which corresponds to $z = 14.5$; the universe has been accelerating since then.

For the ΛCDM model, the acceleration phase can be determined similarly to be beginning at $z = 0.55$.

All the results are summarized in Table 1.

Table 1. The model parameters as determined in the text. The two free parameters of each model, taken from Gupta (2023), are shown in brackets in bold fonts.

Item\Model	**CCC (Base)**	**CCC+TL (Base)**	**CCC (Expanded)**	**CCC+TL (Expanded)**	**LCDM**
Critical density	$3c_0^2(H_0+\alpha)^2/8\pi G_0$	$3c_0^2(H_x+\alpha)^2/8\pi G_0$	$3c_0^2H_0^2/8\pi G_0$	$3c_0^2H_x^2/8\pi G_0$	$3c_0^2H_0^2/8\pi G_0$
$\varepsilon^C_{c,0}/\varepsilon^S_{c,0}$	0.25	0.03	1	0.67	1
$\Omega_{m,0}$	1	1	0.25	0.04	**[0.35]**
$\Omega_{r,0}/\Omega_{m,0}$	3.6×10^{-4}	3.0×10^{-3}	3.6×10^{-4}	3.0×10^{-3}	2.6×10^{-4}
Ω_{de}, Ω_Λ	0	0	0.25	0.64	0.65
$\Omega_{u,0}$	0	0	0.50	0.32	NA
H_0 Km s^{-1}Mpc^{-1}	**[72.7]**	72.6	**[72.7]**	72.6	**[73.0]**
H_x Km s^{-1}Mpc^{-1}	72.7	**[59.5]**	72.7	**[59.5]**	73.0
α/H_x	**[−0.50]**	**[−0.80]**	**[−0.50]**	**[−0.80]**	NA
z at $\Omega_r = \Omega_m$	4600	10,000	4600	10,000	4000
z at $\Omega_m = \Omega_u$	**NA**	**NA**	0.72	10	NA
z at $\Omega_u = \Omega_{de}$	**NA**	**NA**	<0 (future)	1.2	NA
z at $\Omega_m = \Omega_\Lambda$	**NA**	**NA**	NA	NA	0.23
z at acceleration	1.2	14.5	1.2	14.5	0.55

Having shown that dark matter and dark energy are not required in the CCC+TL cosmology, one would want to know how their effect is mitigated in the formation of structures. Without going into detail, we would like to study how some key parameters of structure formation are affected in the absence of dark matter.

4. Concerning Structure Formation

Growth of Matter Perturbations: We will try to determine the ratio of the perturbation amplitudes in CTL (henceforth CTL for brevity) and ΛCDM universes at the epoch of decoupling (redshift $z = 1090$). Let us start with the textbook expression for the matter perturbations [112–114] in a flat ΛCDM universe:

$$\ddot{\delta} + 2H\dot{\delta} = \frac{4\pi G_0}{c_0^2}\bar{\varepsilon}_m\delta. \tag{20}$$

Here, $\bar{\varepsilon}_m$ is the average matter energy density and the perturbation $\delta \equiv (\varepsilon_m - \bar{\varepsilon}_m)/\bar{\varepsilon}_m$. With the density parameter defined as

$$\Omega_m \equiv \frac{\bar{\varepsilon}_m}{\varepsilon_c} = \frac{8\pi G_0 \bar{\varepsilon}_m}{3c_0^2 H^2}, \tag{21}$$

Equation (20) may be written as

$$\ddot{\delta} + 2H\dot{\delta} - \frac{3}{2}\Omega_m H^2 \delta = 0. \tag{22}$$

One can easily derive the perturbation equation for the CTL universe as

$$\ddot{\delta} + 2(H+\alpha)\dot{\delta} - \frac{3}{2}\Omega_m (H+\alpha)^2 \delta = 0, \tag{23}$$

$$\text{with } \Omega_m \equiv \frac{\bar{\varepsilon}_m}{\varepsilon_c} = \frac{8\pi G_0 \bar{\varepsilon}_m}{3c_0^2 (H+\alpha)^2}. \tag{24}$$

In a flat, matter-dominated universe, we have $\Omega_m = 1$. In addition, at the time of recombination, $H \gg |\alpha|$ and α can be ignored. Thus, $H = 2/(3t)$ in both the models. Equations (22) and (23) both reduce to

$$\ddot{\delta} + \frac{4}{3t}\dot{\delta} - \frac{2}{3t^2}\delta = 0. \tag{25}$$

Its general solution is

$$\delta(t) = D_1 t^{2/3} + D_2 t^{-1}. \tag{26}$$

We can ignore the decaying mode, $D_2 t^{-1}$, since it becomes insignificant with increasing t. Parameter D_1 is determined by the initial conditions, which are different in the CTL and ΛCDM models, and so are the expressions for t relating it to scale factor and redshift. Therefore, we will subscript the parameters with Λ and c to identify them for the two models.

We may write the first Friedmann equation for the flat matter-dominated universe at $z \gg 0$ as

$$H_\Lambda = H_{0\Lambda} a_\Lambda^{-3/2};\ H_\mathrm{c} = (H_{0\mathrm{c}} + \alpha) a_c^{-3/2} f_\infty^{-1/2}. \tag{27}$$

Since $H = \dot{a}/a$, their solutions are

$$a_\Lambda = \left(\frac{3H_{0\Lambda}}{2} t\right)^{2/3};\ a_\mathrm{c} = \left(\frac{3(H_{0\mathrm{c}} + \alpha)}{2 f_\infty^{1/2}} t\right)^{2/3}. \tag{28}$$

Therefore,

$$\begin{aligned} \delta_\Lambda(t) &= D_{1\Lambda} t^{2/3} = D_{1\Lambda} \left(\tfrac{3H_{0\Lambda}}{2}\right)^{-2/3} a_\Lambda \\ &= D_{1\Lambda} \left(\tfrac{2}{3H_{0\Lambda}}\right)^{2/3} \tfrac{1}{(1+z_\Lambda)}, \text{ and} \end{aligned} \tag{29}$$

$$\begin{aligned} \delta_\mathrm{c}(t) &= D_{1\mathrm{c}} t^{2/3} = D_{1\mathrm{c}} \left(\tfrac{3(H_{0\mathrm{c}}+\alpha)}{2 f_\infty^{1/2}}\right)^{-2/3} a_\mathrm{c} \\ &= D_{1\mathrm{c}} \left(\tfrac{2 f_\infty^{1/2}}{3(H_{0\mathrm{c}}+\alpha)}\right)^{2/3} \tfrac{1}{(1+z_\mathrm{c})}. \end{aligned} \tag{30}$$

Let us now try to estimate some numbers. Perturbations in the ΛCDM model start to grow from the time of radiation-matter equality, i.e., at $z_{rm} \approx 3440$. It is because matter is primarily dark matter, which does not interact with baryon-photon fluid existing until the time of decoupling at $z_{dec} \approx 1090$. However, in the CTL model, since it has no dark matter, perturbations begin to grow only from the time of decoupling. Since the redshift estimate at the decoupling time is the same in the two models, we can assume $D_{1\Lambda}/D_{1\mathrm{c}} =$

$z_{rm}/z_{dec} = 3.2$. Thus, dark matter dominance in the ΛCDM universe yields a 3.2 advantage over the CTL model on structure formation. Also, we can write in Equations (29) and (30) $1 + z_\Lambda = 1 + z_{dec} = (1 + z_c)(1 + z_t)$. Other parameters are $H_{0\Lambda} = 73$ km s^{-1} Mpc^{-1}, $f_\infty = 3.66$, $H_{0c} = 60$ km s^{-1} Mpc^{-1}, $\alpha = -0.8H_{0c}$, and $1 + z_t = 6.5$ at decoupling. This yields the ratio $\delta_c/\delta_\Lambda \approx 10$ at the time of decoupling; it will be somewhat smaller at later times when galaxies start forming. However, one has to do a numerical solution of the equations involved since many approximations we have made are not valid at lower redshifts when structures begin to form; we have assumed $z \gg 0$. Nevertheless, we do get an idea that the absence of dark matter is not a problem in the CTL model for structure formation when considering the growth of perturbations.

Galaxy Formation: Following Laursen [115], we will try to understand if the galaxies can form in the CTL model, considering that it has no room for dark matter. In the ΛCDM model with dark matter, a cloud of gas and dark matter can become unstable and collapse if it meets Jean's criterion and isolates from the Hubble flow, i.e., from the universe's expansion. Assuming for simplicity spherical symmetry and pressureless gas, the expression for the free-fall time t_{ff} of the cloud is the following [115]:

$$\begin{aligned} t_{ff} &= \left(\frac{3\pi}{32G\rho_m}\right)^{1/2} = \left(\frac{3\pi f_b}{32Gn\overline{m}}\right)^{1/2} \\ &\approx 0.8\,\text{Gyr} \times \left(\frac{n}{10^{-3}\text{cm}^{-3}}\right)^{-1/2}. \end{aligned} \tag{31}$$

Here, ρ_m is the total matter density of the cloud, n is its baryon particle density with mean particle mass $\overline{m}$, and $f_b = \rho_b/\rho_m$ is the baryonic mass fraction determined to be 0.157 by the Planck collaboration [38]. Assuming the same baryon density and cloud temperature in the two models and since $n \sim (1 + z_c)^3 f_c^{-3}$ and $G \sim f_c^3$ in the CTL model and $n \sim (1 + z_\Lambda)^3$ in the ΛCDM model, we obtain the ratio of the free-fall times.

$$R_{ff} \equiv \frac{t_{ffc}}{t_{ff\Lambda}} = \frac{(1 + z_\Lambda)^{3/2}}{(1 + z_c)^{3/2} f_b^{1/2}} = 2.52(1 + z_t)^{3/2}. \tag{32}$$

We are using subscript c for the CTL model rather than x above. At the time of decoupling, $1 + z_t = 6.5$. Therefore, $R_{ff} = 41.7$, which is quite a big disadvantage for the CTL model. However, we need to correct it for Jean density, which for a cloud of mass M is given by

$$\rho_J = \frac{3}{4\pi M^2}\left(\frac{3kT}{G\overline{m}}\right)^3 = \frac{3}{4\pi M^2}\left(\frac{3k_0 T}{G_0 f_c \overline{m}}\right)^3. \tag{33}$$

Since $f_c > 1$, the temperature can be higher in the CTL model by a factor of f_c for the same ρ_J in the ΛCDM model; i.e., clouds can start collapsing at temperature $T' = Tf_c$ in the CTL model rather than at T in the ΛCDM model. Since $T \sim (1 + z) = (1 + z_c)(1 + z_t)$, the temperature $T' \sim (1 + z) f_c(z) \equiv (1 + z') = (1 + z'_c)(1 + z'_t)$. The density gain is then $(1 + z'_c)^3 f(z')^{-3}/\left[(1 + z_c)^3 f(z)^{-3}\right]$. Thus, the Jean density corrected free fall time ratio is

$$R_{ff,J} = 2.52(1 + z_t)^{3/2} \times \left(\frac{(1 + z'_c)^3 f(z')^{-3}}{(1 + z_c)^3 f(z)^{-3}}\right)^{-1/2} \tag{34}$$

This ratio and $R_{ff,J}$ and the base R_{ff} are plotted in Figure 2. Also, we show the age ratio $R_{age} \equiv \text{age}_c/\text{age}_\Lambda$ in Figure 3 derived from [39]. We can see from these two figures that the age advantage in the CTL model over the ΛCDM model overwhelms the free fall time disadvantage by an order of magnitude at higher redshifts where the structures start forming; i.e., there is ample of time in the CTL model to form large scale structures without dark matter.

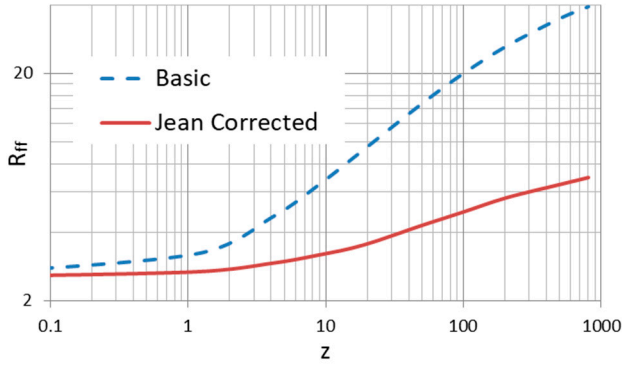

Figure 2. Free fall time ratio for the CTL and ΛCDM models.

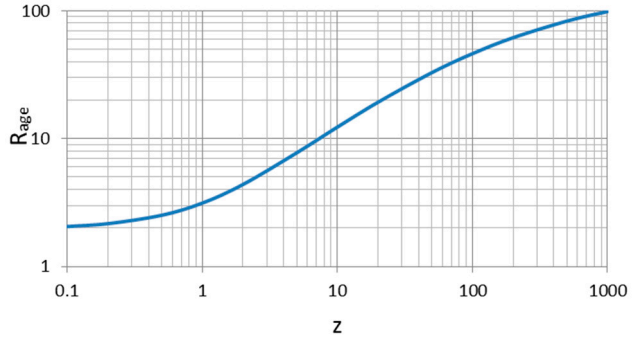

Figure 3. The age advantage in the CTL model over the ΛCDM model.

Next, we consider the virialized parameters (subscript 'vir') of an adiabatically collapsed cloud as the thermal pressure restricts the contraction of the cloud. The shock-heated gas to temperature T_{vir} has mass M_{vir} and radius R_{vir}, which are related (Laursen 2023).

$$T_{vir,\Lambda} = \frac{\overline{m} G_0 M_{vir}}{2 k_0 R_{vir}} \approx 2 \times 10^4 K \times \left(\frac{M_{vir}}{10^8 M_\odot}\right)^{2/3} \left(\frac{1+z}{10}\right). \tag{35}$$

It is assumed that a collapsing cloud reaches an overdensity of 180, and the density that relates mass and radius scales as $(1+z)^3$ in the ΛCDM model. For the CTL model, the equation remains the same except, as discussed above, $(1+z)$ is replaced by $(1+z_c')$. For clarity, let us rewrite the equation:

$$\begin{aligned} T_{vir,c} = \frac{\overline{m} G_0 f^3 M_{vir}}{2 k_0 f^2 R_{vir} f} &\approx 2 \times 10^4 K \times \left(\frac{M_{vir}}{10^8 M_\odot}\right)^{2/3} \left(\frac{1+z_c'}{10}\right) \\ &= T_{vir,\Lambda} \left(\frac{1+z_c'}{1+z}\right). \end{aligned} \tag{36}$$

We show in Figure 4 how the ratio of $1+z$ and $1+z_c'$ vary with redshift z. Their ratio varies within a factor of two. Thus, it is prudent to assume that virialized parameters are not significantly different in the two models, considering the approximation we have used.

Now, we are ready to consider the cooling time of the cloud by radiating its kinetic energy and converting it to thermal energy. The cooling time in terms of cooling function $\Lambda(T)$ is given by [115].

$$\begin{aligned} t_{cool,\Lambda} = \left(\tfrac{3}{2}\right)^5 \frac{k_0 T}{n \Lambda(T)} = 3.3\ Gyr \times &\left(\frac{T}{10^6 K}\right) \left(\frac{n}{10^{-3} \mathrm{cm}^{-3}}\right)^{-1} \\ &\times \left(\frac{\Lambda(T)}{10^{-23} \mathrm{erg\ s^{-1} cm^3}}\right) \end{aligned} \tag{37}$$

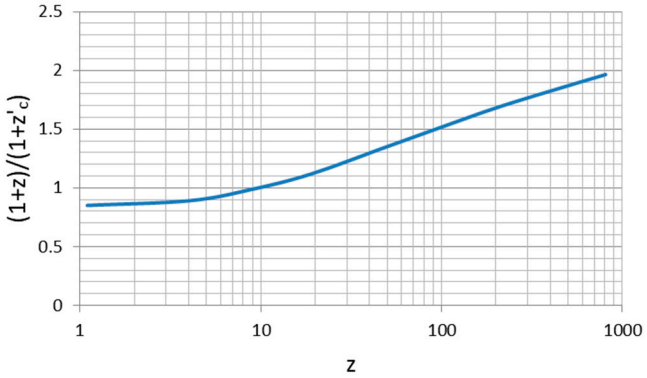

Figure 4. The ratio $(1+z)/(1+z_c')$ as discussed in the text.

Assuming T is about the same for the two models as discussed above, it becomes (length dimension of $\Lambda(T) \sim L^5$, therefore it scales as f^5) for the CTL model.

$$t_{cool,c} = \left(\frac{3}{2}\right)^5 \frac{k_0 f^2 T}{n\prime f^{-3}\Lambda(T) f^5} = \left(\frac{3}{2}\right)^5 \frac{k_0 T}{n\prime \Lambda(T)} = t_{cool,\Lambda} \frac{n}{n\prime},$$

$$R_{cool} \equiv \frac{t_{cool,c}}{t_{cool,\Lambda}} = \frac{n}{n'} = \left(\frac{1+z_c'}{1+z}\right)^3 \tag{38}$$

The ratio of the cooling time in the CTL model and the ΛCDM model R_{cool} as a function of redshift is shown in Figure 5. The cooling is faster in the CTL model up to $z = 10$ and slower at higher redshifts. However, the age advantage of the model greatly offsets any cooling disadvantage by an order of magnitude.

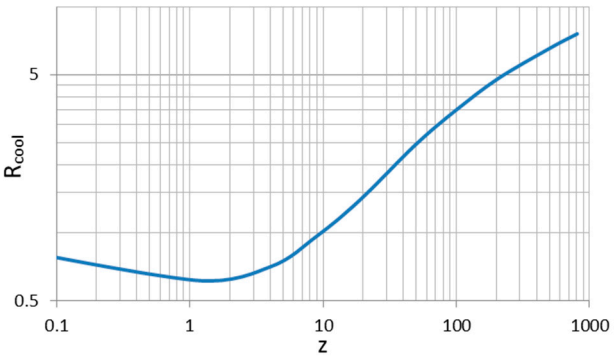

Figure 5. The ratio of cooling time in the CTL and ΛCDM models.

Thus, the formation of structures in the CTL model without dark matter can happen very efficiently due to its age advantage, which starts happening at higher observed redshifts.

Eddington Luminosity: It plays a vital role in the growth of black holes. We may write it with σ_T as the Thomson scattering cross-section,

$$L_E \sim \frac{cG}{\sigma_T} = \frac{c_0 f(z) G_0 f(z)^3}{\sigma_{T,0} f(z)^2} \sim f(z)^2. \tag{39}$$

Since $f(z \gg 0) \to 3.66$, the Eddington luminosity L_E can be up to 13.4 higher in the CTL cosmology than in the ΛCDM cosmology. Thus, one may conclude that black holes can form significantly faster in CTL cosmology. However, since for a luminosity L, the mass accretion rate $\dot{M} \sim Lr/G \sim f^2 f/f^3 = f^0$ is independent of f and thus unaffected by the increase in L_E. Nevertheless, because of the vast age advantage at very high redshifts,

black holes can accrete for up to 100 times longer duration in the CTL cosmology; one does not need super-Eddington luminosity to form supermassive black holes.

5. Discussion

The new cosmological model (CCC+TL) we have analyzed in this paper has intrinsically no dark matter or dark energy in contrast to the same in the ΛCDM model. The critical energy density in the new model is too small to accommodate anything other than the baryonic matter density. It was confirmed by fitting the BAO feature in CMB—the sound horizon angular size; we had to set the whole matter density as baryon density [37]. The unsuccessful search for dark matter and dark energy over many decades may be considered favorable to the CCC+TL cosmology, in which accelerated expansion is caused by *weakening* coupling constants rather than by the elusive dark energy arising from the cosmological constant. However, an apparent ubiquitous recourse to dark matter in explaining multiple astrophysical and cosmological observations may appear difficult to reconcile with the new model and needs careful evaluation. Yet, as discussed in the introduction above, many observations are also inconsistent with dark matter and must be revisited using the CCC+TL model.

The existence of dark matter, necessary in the ΛCDM cosmology, has been of concern for a long time; what exactly is it? All types of baryonic matter add up to no more than about 15% of the ΛCDM matter density obtained by fitting the SNe1a data; i.e., 85% of matter is dark matter. Fitting the CMB temperature anisotropy power spectrum within the ΛCDM paradigm also requires about 85% of matter as non-baryonic matter. All the cosmological models, to our knowledge, that fit SNe1a data acceptably well require dark matter e.g., [116–118], except the CCC+TL model. Since cosmology demanded dark matter, maximum effort was dedicated to explaining astrophysical observations using dark matter; this is true even today. In addition, particle physicists are trying to predict and detect the constituents of the dark matter e.g., [43–45].

Therefore, as discussed in the introduction, alternatives to dark matter, such as MOND, did not have much traction. With the new cosmology that does not require dark matter or dark energy, dark matter alternatives need to be seriously reconsidered e.g., [59,62,119,120] Y. When background cosmology is needed in such studies, one should consider using the CCC+TL model. However, the CCC+TL background is not as straightforward to use as the ΛCDM background. One has to carefully re-derive all the equations needed, especially when time derivatives and time integrals are involved, such as in Christoffel symbols. If applied inappropriately to a problem, the CCC+TL model will yield disappointing results, and one may erroneously reject it. One has to also distinguish between the observable redshift z, which is given by $(1+z) = (1+z_x)(1+z_t)$, and the scale factor $a = 1/(1+z_x)$ in the new model, not $a = 1/(1+z)$. Another tricky thing is to determine z_x for a given z keeping again in mind that $(1+z) = (1+z_x)(1+z_t)$ and that both the redshifts result from covering the same cosmological distance (Equations (35)–(44) in [39]).

When we expand the Friedmann equations in the CCC and CCC+TL models, define the critical density as in the ΛCDM model, i.e., as $\varepsilon^S_{c,0} \equiv 3c_0^2H_0^2/8\pi G_0$, and compare the CCC+TL model with the ΛCDM model (Table 1), we obtain relative energy density numbers for the CCC+TL model as $\Omega_{m,0} = 0.04$, $\Omega_{de} = 0.64$, and $\Omega_{u,0} = 0.32$. We may thus relate Ω_{de} with the dark energy density $\Omega_\Lambda \sim 0.65$ of the ΛCDM model, and $\Omega_{u,0}$ with dark energy interacting with matter, or some form of dark matter, or something unspecified U, and conclude that dark energy and dark matter in the ΛCDM cosmology are manifestations of the varying coupling constants causing the accelerated expansion of the universe moderated by the tired light effect in the CCC+TL cosmology.

It is worth emphasizing that if we consider the CCC model, which also fits the Pantheon+ data as well as the CCC+TL and the ΛCDM models, the critical density, and thus the matter density, turns out to be high enough to require the existence of the dark matter, albeit somewhat less than in the ΛCDM model. However, this is not so for the CCC+TL model, which is the only model that reasonably resolves the 'impossible early galaxy' problem [39],

meaning that, somehow, the tired light effect counters the existence of dark matter. Thus, cosmologically speaking, the tired light effect is equivalent to dark matter!

We will briefly consider the time dilation effect in the CCC and CCC+TL models. Since light follows null geodesic, Equation (1) for the light emitted at a time t_e and detected at the time t_0 in a flat universe yields

$$c_0 \int_{t_e}^{t_0} \frac{dt}{a(t)} = \int_0^r dr. \tag{40}$$

This expression is the same as for the standard FLRW metric since the time dependence of the speed of light determined by $f(t)$ cancels out with the time dependence of distance by the same function. Thus, the time dilation in the CCC model is the same as in the ΛCDM model.

It is not so in the CCC+TL model, as only the expanding universe component of the redshift contributes to the time dilation, i.e., $\delta t_{CTL} \sim (1 + z_X)$. Following Lee [121] and Lewis and Brewer [122], we can write time dilation in terms of the measured redshift z as $\delta t \sim (1 + z)$. Writing $(1 + z_x) = (1 + z)^n$ we have $n = \ln(1 + z_x)/\ln(1 + z)$ with $n = 1$ corresponding to the standard time dilation. Since $(1 + z_x)$ does not vary linearly with $(1 + z)$, n does not have a fixed values; it varies 0.82 to 0.70 in the CCC+TL model (It is worth mentioning that the appropriate time dilation was used in Equation (45) of [39] to fit the redshift vs. distance modulus Pantheon+ data.).

Lee [121] has tried to study the potential variation of the speed of light with redshift using the time dilation broadening of the supernovae type 1a lighting curves by considering $c(z) = c_0(1 + z)^{-b/4}$, i.e., $\delta t \sim (1 + z)^{1-b/4}$. He obtained $b = 0.198 \pm 0.415$ at the 1σ confidence level. With such a large uncertainty and low confidence level, he concluded that the data used was too sparse to yield a meaningful constraint on the variation of the speed of light they were studying (different from the CCC approach). The same would be true for studying the time dilation effect of the tired light, which may also be affected by the stretching of cosmic time in the CCC+TL model [39].

Lewis and Brewer [122] studied 190 quasars through long-term multi-waveband monitoring of their emission over two decades and, using Bayesian analysis, determined $n \equiv 1 - b/4 = 1.28^{+0.28}_{-0.29}$. It contradicts the results of Hawkins [123], who claimed that time dilation is absent in quasars and stated that it is not possible to estimate time dilation reliably from quasar light curves.

A better way in our context is to compare the *aging rate* [121,124], which is the standard time dilation $1/(1 + z)$ for the ΛCDM model, $1/(1 + z_x)$ for the CCC+TL model, and no redshift dependence (constant value unity) for the TL model. Such a comparison against the backdrop of available measured supernovae data is shown in Figure 6. Due to very large error bars in the data, we can only exclude TL as an acceptable model.

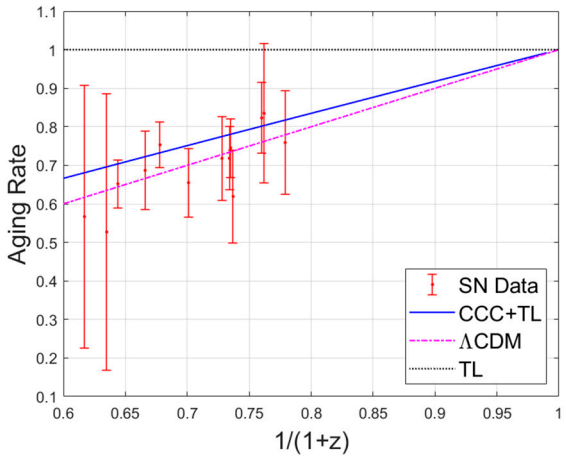

Figure 6. Aging rate comparison in three models shown with supernovae data.

If light curves of the supernovae and quasars could be measured reliably and the evolution of their shapes without time dilation is also established with significantly reduced uncertainty, then they could be used to constrain cosmological models.

A critical contribution of dark matter in cosmology is to provide added gravitational attraction to form baryonic structures within a reasonable time frame. We have shown that the absence of dark matter in the CCC+TL cosmology is not any deterrent in the formation of structures; the age advantage of the new model overwhelms its dark matter disadvantage.

Any new model must faithfully reproduce the CMB power spectrum before it is taken seriously. However, it is the most challenging task to complete reliably, especially in our models, since even the metric is modified. At present, all we have shown using the CCC+TL model [37] is that (a) the model is consistent with the angular size of baryonic acoustic oscillations in CMB, and (b) the black body spectrum of CMB is preserved. Nevertheless, it gives us the confidence to put in the effort and resources needed to accomplish the task. Our effort is continuing with experts in the field to modify existing Boltzmann codes, such as CLASS [125] and CAMB [126].

The evolution of the blackbody spectrum of photons in the CCC+TL model was determined in an earlier paper (Equations (19)–(23) of [37]). It was shown that the CMB emission has the black body spectrum with its intensity scaling as $(1 + z_t)^{-3}$ due to tired light. Since $z_t = 0$ at present, there is no tired light effect on the measured intensity of the spectrum.

A significant effort has been put into measuring the variation of the coupling constants with essentially negative results (e.g., citations 1–30 in [111]). Let us see why we obtain negative results: As the universe expands, its macroscopic length scale evolves as given by the scale factor $a(t)$. Similarly, one could expect the length dimension in the constants to evolve at the microscopic scale as provided by another scale factor represented by the function $f(t)$. Considering then the length dimension in various constants, we can see why $G \sim f^3$, $c \sim f$, $h \sim f^2$, $k_B \sim f^2$, etc., and why dimensionless constants, like the fine structure constant, do not appear to evolve on the cosmological time scale.

To be specific, we are considering two scaling factors: $a(t)$ for the expansion of the universe's space and $f(t)$ for the length dimension of the constants as well as the length unit itself. Neither $a(t)$ nor $f(t)$ applies to the tired light component of the hybrid model. In the CCC+TL model, the redshift is mostly due to expanding space, as in the ΛCDM and the CCC models. Only a fraction of the redshift is due to the tired light effect of unknown origin in the CCC+TL model. The ratio of the two redshifts against total redshift was reported graphically in Figure 6 of [39]. The function $f(t)$ can also be considered as defining a universal clock having the same value everywhere, irrespective of local conditions. Thus, there is no change in frequency associated with an energy level transition due to evolving $f(t)$; the change is only due to $a(t)$; i.e., due only to the expansion of space. Thus, the frequency change happens only in the CCC component of the CCC+TL model since space expands only in the CCC model. The TL frequency change is unrelated to $f(t)$ or $a(t)$.

One cannot even measure an evolving dimensionful constant, such as $G(t)$, because in such measurements, invariably, one keeps the other dimensionful constants to remain fixed, i.e., constraints $f(t)$ as constant. It automatically constrains the constant selected for studying its variation to its current value; one cannot measure the variation of a constant unless all others are allowed to vary simultaneously. The effort should therefore be on the measurement of $f(t)$ rather than on the variation of a particular constant. The real challenge is to think of an experiment that can measure the variation of $f(t)$, i.e., $f(z)$.

Next, we need to find a way of isolating and measuring the two redshifts: (1) due to the expansion of the universe and (2) due to the tired light effect. Wang et al. [127,128] proposed a method of testing redshift drift, a direct measure of cosmological expansion, using gravitationally lensed images of distant objects. Multiple images arriving at the same instant would travel different distances and thus would have left an object at different times. If a high enough accuracy can be achieved in measuring redshifts, one could

estimate the redshift difference using any two images, hence the cosmological expansion. Any observed difference could be due to the redshift drift, the tired light effect, or both. Another gravitational lensing method uses SNe1a with a well-defined brightness-peaking profile or quasars with some brightness fluctuation profile marker [129–131]. Such markers in their luminosity show up at different times in their images; different path lengths would mean different contributions to the redshift due to the tired light effect, while the redshift due to the expansion would be the same in such images. However, the redshift difference would be too small to be measurable by current technology; for a difference of one year in the arrival time of two images, the redshift difference is expected to be $\sim 10^{-9}$.

Finally, we should consider the coincidence problem in the context of the CCC and CCC+TL models. We can consider it in two ways: (i) These models have no dark energy per se. So, the coincidence problem becomes meaningless. In the CCC+TL model, there is no dark matter either since the critical density is too small to accommodate anything but the baryonic matter. (ii) When we compare these models with the ΛCDM model, we relate α^2 to $\Lambda/3$ and have an 'unknown' term involving α. Therefore, the origin of energy densities corresponding to both terms is the varying coupling constants. So, it is not a surprise that their values are not too different, meaning again that there is no coincidence problem.

6. Conclusions

We have shown that the CCC+TL model, which nicely fits the Pantheon+ data, amicably resolves the 'impossible early galaxy' problem, and adequately reproduces the BAO features in the galaxy distribution and the cosmic microwave background, eliminatesg the need for dark matter. We have established that dark energy and dark matter of the standard ΛCDM model are not arbitrary, but a reflection of the evolutionary nature of coupling constants anticipated originally by Dirac in 1937. Also, we have shown that structures can effectively form in the CCC+TL universe without dark matter due primarily to its age advantage over the ΛCDM universe. It remains to be shown how the new model complies with other observations, such as the CMB anisotropy power spectrum and BBN element abundances, reproduces various structure formations, and explains the galaxy rotations curves, gravitational lensing abnormalities, etc. Until then, the new model is just another alternative cosmological model. Finally, could the U energy density do the job of dark matter?

Funding: This research work was partially funded by Macronix Research Corporation.

Data Availability Statement: References have been provided for the data used in this work.

Acknowledgments: The author is grateful to Rodrigo Cuzinatto, Pedro Pompeia, Utkarsh Kumar, and Piyush Singhal for helpful discussions, and to Brian Keating, Avi Loeb, Nikita Lovyagin, David Spergel, and Ethan Vishniac for their communications and constructive critical comments on the CCC+TL model. He wishes to convey his appreciation to reviewers of the paper whose critical assessment of the paper's manuscripts led to its significant improvement. Finally, he is thankful to Macronix Research Corporation for the unconditional research grant for this work.

Conflicts of Interest: The authors declare that this study received partial funding in the form of a research grant from Macronix Research Corporation. The funder was not involved in the study design, collection, analysis, interpretation of data, the writing of this article or the decision to submit it for publication.

References

1. Riess, A.G.; Filippenko, A.V.; Challis, P.; Clocchiatti, A.; Diercks, A.; Garnavich, P.M.; Gilliland, R.L.; Hogan, C.J.; Jha, S.; Kirshner, R.P.; et al. Observational Evidence from Supernovae for an Accelerating Universe and a Cosmological Constant. *Astron. J.* **1998**, *116*, 1009–1038. [CrossRef]
2. Perlmutter, S.; Aldering, G.; Goldhaber, G.; Knop, R.A.; Nugent, P.; Castro, P.G.; Deustua, S.; Fabbro, S.; Goobar, A.; Groom, D.E.; et al. Measurements of Ω and Λ from 42 High-Redshift Supernovae. *Astrophys. J.* **1999**, *517*, 565. [CrossRef]
3. Jimenez, R.; Loeb, A. Constraining Cosmological Parameters Based on Relative Galaxy Ages. *Astrophys. J.* **2002**, *573*, 37–42. [CrossRef]

4. Eisenstein, D.J.; Zehavi, I.; Hogg, D.W.; Scoccimarro, R.; Blanton, M.R.; Nichol, R.C.; Scranton, R.; Seo, H.; Tegmark, M.; Zheng, Z.; et al. Detection of the Baryon Acoustic Peak in the Large-Scale Correlation Function of SDSS Luminous Red Galaxies. *Astrophys. J.* **2005**, *633*, 560–574. [CrossRef]
5. Betoule, M.; Kessler, R.; Guy, J.; Mosher, J.; Hardin, D.; Biswas, R.; Astier, P.; El-Hage, P.; Konig, M.; Kuhlmann, S.; et al. Improved cosmological constraints from a joint analysis of the SDSS-II and SNLS supernova samples. *Astron. Astrophys.* **2014**, *568*, A22. [CrossRef]
6. Haridasu, B.S.; Lukovi ć, V.V.; D'agostino, R.; Vittorio, N. Strong evidence for an accelerating Universe. *Astron. Astrophys.* **2017**, *600*, L1. [CrossRef]
7. Bahcall, N.A. Dark matter universe. *Proc. Natl. Acad. Sci. USA* **2015**, *112*, 12243. [CrossRef] [PubMed]
8. Weinberg, D.H.; Bullock, J.S.; Governato, F.; de Naray, R.K.; Peter, A.H.G. Cold dark matter: Controversies on small scales. *Proc. Natl. Acad. Sci. USA* **2015**, *112*, 12249–12255. [CrossRef] [PubMed]
9. Yang, M.; Zhu, L.; Lei, Y.; Boardman, N.; Weijmans, A.M.; Morganti, R.; Oosterloo, T.; Duc, P.A. Dark matter measurements combining stellar and HI kinematics: 30% $1-\sigma$ outliers with low dark matter content at 5Re. *Mon. Not. R. Astron. Soc.* **2024**, *528*, 5295–5308. [CrossRef]
10. Boylan-Kolchin, M.; Bullock, J.S.; Kaplinghat, M. Too big to fail? The puzzling darkness of massive Milky Way subhaloes. *Mon. Not. R. Astron. Soc. Lett.* **2011**, *415*, L40–L44. [CrossRef]
11. Navarro, J.F.; Frenk, C.S.; White, S.D.M. A Universal Density Profile from Hierarchical Clustering. *Astrophys. J.* **1997**, *490*, 493–508. [CrossRef]
12. Bunker, A.J.; Saxena, A.; Cameron, A.J.; Willott, C.J.; Curtis-Lake, E.; Jakobsen, P.; Carniani, S.; Smit, R.; Maiolino, R.; Witstok, J.; et al. JADES NIRSpec Spectroscopy of GN-z11: Lyman-α emission and possible enhanced nitrogen abundance in a z = 10.60 luminous galaxy. *Astron. Astrophys.* **2023**, *677*, A88. [CrossRef]
13. Goerdt, T.; Moore, B.; Read, J.I.; Stadel, J.; Zemp, M. Does the Fornax dwarf spheroidal have a central cusp or core? *Mon. Not. R. Astron. Soc.* **2006**, *368*, 1073–1077. [CrossRef]
14. Klypin, A.; Kravtsov, A.V.; Valenzuela, O.; Prada, F. Where are the missing galactic satellites? *Astrophys. J.* **1999**, *522*, 82–92. [CrossRef]
15. Lord, K. *Baltimore Lectures on Molecular Dynamics and the Wave Theory of Light*; C.J. Clay and Sons: London, UK, 1904; p. 274.
16. Zwicky, F. Republication of: The redshift of extragalactic nebulae. *Gen. Relativ. Gravit.* **2009**, *41*, 207–224. [CrossRef]
17. Rubin, V.C.; Ford, W.K., Jr. Rotation of the Andromeda Nebula from a Spectroscopic Survey of Emission Regions. *Astrophys. J.* **1970**, *150*, 379. [CrossRef]
18. Rubin, V.C.; Ford, W.K., Jr.; Thonnard, N. Extended rotation curves of high-luminosity spiral galaxies. IV. Systematic dynamical properties, Sa through Sc. *Astrophys. J.* **1978**, *225*, L107–L111. [CrossRef]
19. Bosma, A. 21-cm line studies of spiral galaxies. II. The distribution and kinematics of neutral hydrogen in spiral galaxies of various morphological types. *Astron. J.* **1981**, *86*, 1825–1846. [CrossRef]
20. Sofue, Y.; Rubin, V. Rotation Curves of Spiral Galaxies. Annu. Rev. *Astron. Astrophys.* **2001**, *39*, 137–174. [CrossRef]
21. De Blok, W.J.; Walter, F.; Brinks, E.; Trachternach, C.; Oh, S.H.; Kennicutt, R.C. High-Resolution Rotation Curves and Galaxy Mass Models from THINGS. *Astron. J.* **2008**, *136*, 2648. [CrossRef]
22. Genzel, R.; Schreiber, N.M.F.; Übler, H.; Lang, P.; Naab, T.; Bender, R.; Tacconi, L.J.; Wisnioski, E.; Wuyts, S.; Alexander, T.; et al. Strongly baryon-dominated disk galaxies at the peak of galaxy formation ten billion years ago. *Nature* **2017**, *543*, 397–401. [CrossRef]
23. Lang, P.; Schreiber, N.M.F.; Genzel, R.; Wuyts, S.; Wisnioski, E.; Beifiori, A.; Belli, S.; Bender, R.; Brammer, G.; Burkert, A.; et al. Falling outer rotation curves of star-forming galaxies at $0.6 \lesssim Z \lesssim 2.6$ probed with KMOS3D and SINS/ZC-SINF. *Astrophys. J.* **2017**, *840*, 92. [CrossRef]
24. Nelson, A.; Williams, P. Recent Observations of the Rotation of Distant Galaxies and the Implication for Dark Matter. *arXiv* **2024**, arXiv:2401.13783. [CrossRef]
25. Faber, S.M.; Jackson, R.E. Velocity dispersions and mass-to-light ratios for elliptical galaxies. *Astrophys. J.* **1976**, *204*, 668–683. [CrossRef]
26. Binny, J.; Merrifield, M. *Galactic Astronomy*; Princeton University Press: Princeton, NJ, USA, 1998; p. 712.
27. Allen, S.W.; Evrard, A.E.; Mantz, A.B. Cosmological Parameters from Observations of Galaxy Clusters. *Annu. Rev. Astron. Astrophys.* **2011**, *49*, 409–470. [CrossRef]
28. Taylor, A.N.; Dye, S.; Broadhurst, T.J.; Benitez, N.; van Kampen, E. Gravitational Lens Magnification and the Mass of Abell 1689. *Astrophys. J.* **1998**, *501*, 539–553. [CrossRef]
29. Natarajan, P.; Chadayammuri, U.; Jauzac, M.; Richard, J.; Kneib, J.-P.; Ebeling, H.; Jiang, F.; Bosch, F.v.D.; Limousin, M.; Jullo, E.; et al. Mapping substructure in the HST Frontier Fields cluster lenses and in cosmological simulations. *Mon. Not. R. Astron. Soc.* **2017**, *468*, 1962–1980. [CrossRef]
30. Hinshaw, G.; Weiland, J.L.; Hill, R.S.; Odegard, N.; Larson, D.; Bennett, C.L.; Dunkley, J.; Gold, B.; Greason, M.R.; Jarosik, N.; et al. Five-Year Wilkinson Microwave Anisotropy Probe (WMAP) Observations: Data Processing, Sky Maps, and Basic Results. *Astrophys. J. Suppl. Ser.* **2009**, *180*, 225. [CrossRef]
31. Ade, P.A.; Aghanim, N.; Arnaud, M.; Ashdown, M.; Aumont, J.; Baccigalupi, C.; Banday, A.J.; Barreiro, R.B.; Bartlett, J.G.; Bartolo, N.; et al. Planck 2015 results. XIII. Cosmological parameters. *Astron. Astrophys.* **2016**, *594*, A13.

32. Schramm, D.N. The age of the universe, dark matter, and structure formation. *Proc. Natl. Acad. Sci. USA* **1998**, *95*, 1. [CrossRef]
33. Popolo, A.D. Dark matter and structure formation a review. *Astron. Rep.* **2007**, *51*, 169–196. [CrossRef]
34. Mina, M.; Mota, D.F.; Winther, H.A. Solitons in the dark: First approach to non-linear structure formation with fuzzy dark matter. *Astron. Astrophys.* **2022**, *662*, A29. [CrossRef]
35. Clowe, D.; Bradač, M.; Gonzalez, A.H.; Markevitch, M.; Randall, S.W.; Jones, C.; Zaritsky, D. A direct empirical proof of the existence of dark matter. *Astrophys. J.* **2006**, *648*, L109–L113. [CrossRef]
36. Ding, Z.; Seo, H.-J.; Huff, E.; Saito, S.; Clowe, D. Detecting baryon acoustic oscillations in dark matter from kinematic weak lensing surveys. *Mon. Not. R. Astron. Soc.* **2019**, *487*, 253–267. [CrossRef]
37. Gupta, R.P. Testing CCC+TL Cosmology with Observed BAO Features. *arXiv* **2024**, arXiv:2401.09483.
38. Aghanim, N.; Akrami, Y.; Ashdown, M.; Aumont, J.; Baccigalupi, C.; Ballardini, M.; Banday, A.J.; Barreiro, R.B.; Bartolo, N.; Basak, S.; et al. [Planck Collaboration] Planck 2018 results. VI. Cosmological parameters. *Astron. Astrophys.* **2020**, *641*, A6.
39. Gupta, R.P. JWST early Universe observations and ΛCDM cosmology. *Mon. Not. R. Astron. Soc.* **2023**, *524*, 3385–3395. [CrossRef]
40. Chae, K.-H.; Lelli, F.; Desmond, H.; McGaugh, S.S.; Li, P.; Schombert, J.M. Testing the Strong Equivalence Principle: Detection of the External Field Effect in Rotationally Supported Galaxies. *Astrophys. J.* **2020**, *904*, 51. [CrossRef]
41. Nadler, E.O.; Yang, D.; Yu, H.-B. A Self-interacting Dark Matter Solution to the Extreme Diversity of Low-mass Halo Properties. *Astrophys. J.* **2023**, *958*, L39. [CrossRef]
42. Bose, B.; Carrilho, P.; Marinucci, M.; Moretti, C.; Pietroni, M.; Carella, E.; Piga, L.; Wright, B.S.; Vernizzi, F.; Carbone, C.; et al. [Euclid Collaboration] Euclid preparation. Modelling spectroscopic clustering on mildly nonlinear scales in beyond-ΛCDM models. *arXiv* **2023**, arXiv:2311.13529.
43. Adhikari, P.; Ajaj, R.; Alpízar-Venegas, M.; Auty, D.J.; Benmansour, H.; Bina, C.E.; Bonivento, W.; Boulay, M.G.; Cadeddu, M.; Cai, B.; et al. First Direct Detection Constraints on Planck-Scale Mass Dark Matter with Multiple-Scatter Signatures Using the DEAP-3600 Detector. *Phys. Rev. Lett.* **2022**, *128*, 011801. [CrossRef]
44. Kane, G.; Watson, S. Dark matter and LHC: What is the connection? *Mod. Phys. Lett. A* **2008**, *23*, 2103–2123. [CrossRef]
45. Fox, P.J.; Harnik, R.; Kopp, J.; Tsai, Y. LEP shines light on dark matter. *Phys. Rev. D* **2011**, *84*, 014028. [CrossRef]
46. Mannheim, P.D. Alternatives to Dark Matter and Dark Energy Prog. *Part. Nucl. Phys.* **2006**, *56*, 340–445. [CrossRef]
47. Milgrom, M. A modification of the Newtonian dynamics as a possible alternative to the hidden mass hypothesis. *Astrophys. J.* **1983**, *270*, 365–370. [CrossRef]
48. Milgrom, M. Universal Modified Newtonian Dynamics Relation between the Baryonic and "Dynamical" Central Surface Densities of Disc Galaxies. *Phys. Rev. Lett.* **2016**, *117*, 141101. [CrossRef]
49. Milgrom, M. MOND in galaxy groups: A superior sample. *Phys. Rev. D* **2019**, *99*, 044041. [CrossRef]
50. Milgrom, M. MOND vs. dark matter in light of historical parallels. *Stud. Hist. Philos. Sci. Part B Stud. Hist. Philos. Mod. Phys.* **2020**, *71*, 170–195. [CrossRef]
51. Kroupa, P. A modern view of galaxies and their stellar populations. *arXiv* **2023**, arXiv:2310.01473.
52. Milgrom, M. MOND as manifestation of modified inertia. *arXiv* **2023**, arXiv:2310.14334.
53. Kroupa, P.; Pawlowski, M.; Milgrom, M. The failures of the standard model of cosmology require a new paradigm. *Int. J. Mod. Phys. D* **2012**, *21*, 1230003. [CrossRef]
54. Capozziello, S.; De Laurentis, M. The dark matter problem from f(R) gravity viewpoint. *Ann. der Phys.* **2012**, *524*, 545–578. [CrossRef]
55. Farnes, J.S. A unifying Theory of Dark Energy and Dark Matter: Negative Masses and Matter Creation within a Modified ΛCDM Framework. *Astron. Astrophys.* **2018**, *620*, A92. [CrossRef]
56. Verlinde, E. On the Origin of Gravity and the Laws of Newton. *J. High Energy Phys.* **2011**, *2011*, 29. [CrossRef]
57. Gonzalo, E.; Montero, M.; Obied, G.; Vafa, C. Dark Dimension Gravitons as Dark Matter. *J. High Energy Phys.* **2023**, *2023*, 109. [CrossRef]
58. Yahalom, A. The Geometrical Meaning of Time. *Found. Phys.* **2008**, *38*, 489–497. [CrossRef]
59. Yahalom, A. The Effect of Retardation on Galactic Rotation Curves. *J. Phys. Conf. Ser.* **2019**, *1239*, 012006. [CrossRef]
60. Wagman, M.; Horwitz, L.P.; Yahalom, A. Applying Retardation Theory to Galaxies. *J. Phys. Conf. Ser.* **2023**, *2482*, 012005. [CrossRef]
61. Joyce, A.; Jain, B.; Khoury, J.; Trodden, M. Beyond the Cosmological Standard Model. *Phys. Rep.* **2015**, *568*, 1–98. [CrossRef]
62. Skordis, C.; Złośnik, T. New Relativistic Theory for Modified Newtonian Dynamics. *Phys. Rev. Lett.* **2021**, *127*, 161302. [CrossRef] [PubMed]
63. Naidu, R.P.; Oesch, P.A.; van Dokkum, P.; Nelson, E.J.; Suess, K.A.; Brammer, G.; Whitaker, K.E.; Illingworth, G.; Bouwens, R.; Tacchella, S.; et al. Two remarkably luminous galaxy candidates at z ≈ 10–12 revealed by JWST. *Astrophys. J. Lett.* **2022**, *940*, L14. [CrossRef]
64. Naidu, R.P.; Oesch, P.A.; Setton, D.J.; Matthee, J.; Conroy, C.; Johnson, B.D.; Weaver, J.R.; Bouwens, R.J.; Brammer, G.B.; Dayal, P.; et al. Schrodinger's Galaxy Candidate: Puzzlingly Luminous at z ≈ 17, or Dusty/Quenched at z ≈ 5? *arXiv* **2022**, arXiv:2208.02794.
65. Labbé, I.; van Dokkum, P.; Nelson, E.; Bezanson, R.; Suess, K.A.; Leja, J.; Brammer, G.; Whitaker, K.; Mathews, E.; Stefanon, M.; et al. A population of red candidate massive galaxies ~600 Myr after the Big Bang. *Nature* **2023**, *616*, 266–269. [CrossRef] [PubMed]

66. Curtis-Lake, E.; Carniani, S.; Cameron, A.; Charlot, S.; Jakobsen, P.; Maiolino, R.; Bunker, A.; Witstok, J.; Smit, R.; Chevallard, J.; et al. Spectroscopic confirmation of four metal-poor galaxies at z = 10.3–13.2. *Nat. Astron.* **2023**, *7*, 622–632. [CrossRef]
67. Hainline, K.N.; Johnson, B.D.; Robertson, B.; Tacchella, S.; Helton, J.M.; Sun, F.; Eisenstein, D.J.; Simmonds, C.; Topping, M.W.; Whitler, L.; et al. The Cosmos in Its Infancy: JADES Galaxy Candidates at z > 8 in GOODS-S and GOODS-N. *Astrophys. J.* **2024**, *964*, 71. [CrossRef]
68. Robertson, B.E.; Tacchella, S.; Johnson, B.D.; Hainline, K.; Whitler, L.; Eisenstein, D.J.; Endsley, R.; Rieke, M.; Stark, D.P.; Alberts, S.; et al. Identification and properties of intense star-forming galaxies at redshifts z > 10. *Nat. Astron.* **2023**, *7*, 611–621. [CrossRef]
69. Adams, N.J.; Conselice, C.J.; Ferreira, L.; Austin, D.; Trussler, J.A.; Juodžbalis, I.; Wilkins, S.M.; Caruana, J.; Dayal, P.; Verma, A.; et al. Discovery and properties of ultra-high redshift galaxies (9 < z < 12) in the JWST ERO SMACS 0723 Field. *Mon. Not. R. Astron. Soc.* **2023**, *518*, 4755–4766.
70. Atek, H.; Chemerynska, I.; Wang, B.; Furtak, L.J.; Weibel, A.; Oesch, P.; Weaver, J.R.; Labbé, I.; Bezanson, R.; van Dokkum, P.; et al. JWST UNCOVER: Discovery of z > 9 Galaxy Candidates behind the Lensing Cluster Abell 2744. *Mon. Not. R. Astron. Soc.* **2023**, *524*, 5486–5496. [CrossRef]
71. Chen, Z.; Stark, D.P.; Endsley, R.; Topping, M.; Whitler, L.; Charlot, S. JWST/NIRCam Observations of Stars and HII Regions in z $\sim eq$ 6−8 Galaxies: Properties of Star Forming Complexes on 150 pc Scales. *Mon. Not. R. Astron. Soc.* **2022**, *518*, 5607–5619. [CrossRef]
72. Donnan, C.T.; McLeod, D.J.; Dunlop, J.S.; McLure, R.J.; Carnall, A.C.; Begley, R.; Cullen, F.; Hamadouche, M.L.; Bowler, R.A.; Magee, D.; et al. The evolution of the galaxy UV luminosity function at redshifts z $\sim eq$ 8–15 from deep JWST and ground-based near-infrared imaging. *Mon. Not. R. Astron. Soc.* **2022**, *518*, 6011–6040. [CrossRef]
73. Finkelstein, S.L.; Bagley, M.B.; Haro, P.A.; Dickinson, M.; Ferguson, H.C.; Kartaltepe, J.S.; Papovich, C.; Burgarella, D.; Kocevski, D.D.; Iyer, K.G.; et al. A Long Time Ago in a Galaxy Far, Far Away: A Candidate z∼12 Galaxy in Early JWST CEERS Imaging. *Astrophys. J. Lett.* **2022**, *940*, L55. [CrossRef]
74. Ono, Y.; Harikane, Y.; Ouchi, M.; Yajima, H.; Abe, M.; Isobe, Y.; Shibuya, T.; Wise, J.H.; Zhang, Y.; Nakajima, K.; et al. Morphologies of Galaxies at z $\gtrsim$ 9 Uncovered by JWST/NIRCam Imaging: Cosmic Size Evolution and an Identification of an Extremely Compact Bright Galaxy at z∼12. *Astrophys. J.* **2023**, *951*, 72. [CrossRef]
75. Tacchella, S.; Eisenstein, D.J.; Hainline, K.; Johnson, B.D.; Baker, W.M.; Helton, J.M.; Robertson, B.; Suess, K.A.; Chen, Z.; Nelson, E.; et al. JADES Imaging of GN-z11: Revealing the Morphology and Environment of a Luminous Galaxy 430 Myr after the Big Bang. *Astrophys. J.* **2023**, *952*, 74. [CrossRef]
76. Tacchella, S.; Johnson, B.D.; Robertson, B.E.; Carniani, S.; D'eugenio, F.; Kumari, N.; Maiolino, R.; Nelson, E.J.; Suess, K.A.; Übler, H.; et al. JWST NIRCam + NIRSpec: Interstellar medium and stellar populations of young galaxies with rising star formation and evolving gas reservoirs. *Mon. Not. R. Astron. Soc.* **2023**, *522*, 6236–6249. [CrossRef]
77. Wu, Y.; Cai, Z.; Sun, F.; Bian, F.; Lin, X.; Li, Z.; Li, M.; Bauer, F.E.; Egami, E.; Fan, X.; et al. The Identification of a Dusty Multiarm Spiral Galaxy at z = 3.06 with JWST and ALMA. *Astrophys. J. Lett.* **2022**, *942*, L1. [CrossRef]
78. Yang, L.; Morishita, T.; Leethochawalit, N.; Castellano, M.; Calabro, A.; Treu, T.; Bonchi, A.; Fontana, A.; Mason, C.; Merlin, E.; et al. Early Results from GLASS-JWST. V: The First Rest-frame Optical Size–Luminosity Relation of Galaxies at z > 7. *Astrophys. J. Lett.* **2022**, *938*, L17. [CrossRef]
79. Austin, D.; Adams, N.; Conselice, C.J.; Harvey, T.; Ormerod, K.; Trussler, J.; Li, Q.; Ferreira, L.; Dayal, P.; Juodžbalis, I. A Large Population of Faint 8 < z < 16 Galaxies Found in the First JWST NIRCam Observations of the NGDEEP Survey. *Astrophys. J.* **2023**, *952*, L7. [CrossRef]
80. Baggen, J.F.; van Dokkum, P.; Labbé, I.; Brammer, G.; Miller, T.B.; Bezanson, R.; Leja, J.; Wang, B.; Whitaker, K.E.; Suess, K.A.; et al. Sizes and mass profiles of candidate massive galaxies discovered by JWST at 7 < z < 9: Evidence for very early formation of the central ~100 pc of present-day ellipticals. *Astrophys. J. Lett.* **2023**, *955*, L12.
81. Haslbauer, M.; Kroupa, P.; Zonoozi, A.H.; Haghi, H. Has JWST Already Falsified Dark-matter-driven Galaxy Formation? *Astrophys. J.* **2022**, *939*, L31. [CrossRef]
82. Inayoshi, K.; Harikane, Y.; Inoue, A.K.; Li, W.; Ho, L.C. A Lower Bound of Star Formation Activity in Ultra-high-redshift Galaxies Detected with JWST: Implications for Stellar Populations and Radiation Sources. *Astrophys. J.* **2022**, *938*, L10. [CrossRef]
83. Kannan, R.; Springel, V.; Hernquist, L.; Pakmor, R.; Delgado, A.M.; Hadzhiyska, B.; Hernández-Aguayo, C.; Barrera, M.; Ferlito, F.; Bose, S.; et al. The MillenniumTNG Project: The galaxy population at z $\geq$ 8. *Mon. Not. R. Astron. Soc.* **2023**, *524*, 2594–2605. [CrossRef]
84. Keller, B.W.; Munshi, F.; Trebitsch, M.; Tremmel, M. Can Cosmological Simulations Reproduce the Spectroscopically Confirmed Galaxies Seen at z $\geq$ 10? *Astrophys. J.* **2023**, *943*, L28. [CrossRef]
85. Regan, J. Massive Star Formation in Overdense Regions of the Early Universe. *arXiv* **2022**, arXiv:2210.04899. [CrossRef]
86. Yajima, H.; Abe, M.; Fukushima, H.; Ono, Y.; Harikane, Y.; Ouchi, M.; Hashimoto, T.; Khochfar, S. FOREVER22: The first bright galaxies with population III stars at redshifts z $\sim eq$ 10–20 and comparisons with JWST data. *Mon. Not. R. Astron. Soc.* **2023**, *525*, 4832–4839. [CrossRef]
87. Mason, C.A.; Trenti, M.; Treu, T. The brightest galaxies at cosmic dawn. *Mon. Not. R. Astron. Soc.* **2023**, *521*, 497–503. [CrossRef]
88. Mirocha, J.; Furlanetto, S.R. Balancing the efficiency and stochasticity of star formation with dust extinction in z $\gtrsim$ 10 galaxies observed by JWST. *Mon. Not. R. Astron. Soc.* **2022**, *519*, 843–853. [CrossRef]

89. Whitler, L.; Stark, D.P.; Endsley, R.; Chen, Z.; Mason, C.; Topping, M.W.; Charlot, S. Insight from JWST/NIRCam into galaxy overdensities around bright Lyα emitters during reionization: Implications for ionized bubbles at z$\sim$9. *Mon. Not. R. Astron. Soc.* **2023**, *529*, 855–872. [CrossRef]
90. Whitler, L.; Endsley, R.; Stark, D.P.; Topping, M.; Chen, Z.; Charlot, S. On the ages of bright galaxies $\sim$500 Myr after the big bang. *Mon. Not. R. Astron. Soc.* **2023**, *519*, 157–171. [CrossRef]
91. McCaffrey, J.; Hardin, S.; Wise, J.H.; Regan, J.A. No Tension: JWST Galaxies at z > 10 Consistent with Cosmological Simulations. *arXiv* **2023**, arXiv:2304.13755. [CrossRef]
92. Ellis, R.S. *When Galaxies Were Born: The Quest for Cosmic Dawn*; Princeton University Press: Princeton, NJ, USA, 2022.
93. Reinoso, B.; Klessen, R.S.; Schleicher, D.; Glover, S.C.O.; Solar, P. Formation of supermassive stars in the first star clusters. *Mon. Not. R. Astron. Soc.* **2023**, *521*, 3553–3569. [CrossRef]
94. Brummel-Smith, C.; Skinner, D.; Sethuram, S.S.; Wise, J.H.; Xia, B.; Taori, K. Inferred galaxy properties during Cosmic Dawn from early JWST photometry results. *Mon. Not. R. Astron. Soc.* **2023**, *525*, 4405–4425. [CrossRef]
95. Dolgov, A.D. James Webb Space Telescope: Data, problems, and resolution. *arXiv* **2023**, arXiv:2301.01365.
96. Larson, R.L.; Finkelstein, S.L.; Kocevski, D.D.; Hutchison, T.A.; Trump, J.R.; Haro, P.A.; Bromm, V.; Cleri, N.J.; Dickinson, M.; Fujimoto, S.; et al. A CEERS Discovery of an Accreting Supermassive Black Hole 570 Myr after the Big Bang: Identifying a Progenitor of Massive z > 6 Quasars. *Astrophys. J. Lett.* **2023**, *953*, L29. [CrossRef]
97. Maiolino, R.; Scholtz, J.; Witstok, J.; Carniani, S.; D'Eugenio, F.; de Graaff, A.; Übler, H.; Tacchella, S.; Curtis-Lake, E.; Arribas, S.; et al. A small and vigorous black hole in the early Universe. *Nature* **2024**, *627*, 59–63. [CrossRef] [PubMed]
98. Dekel, A.; Sarkar, K.C.; Birnboim, Y.; Mandelker, N.; Li, Z. Efficient Formation of Massive Galaxies at Cosmic Dawn by Feedback-Free Starbursts. *Mon. Not. R. Astron. Soc.* **2023**, *523*, 3201–3218. [CrossRef]
99. Boyett, K.; Trenti, M.; Leethochawalit, N.; Calabró, A.; Metha, B.; Roberts-Borsani, G.; Dalmasso, N.; Yang, L.; Santini, P.; Treu, T.; et al. A massive interacting galaxy 510 million years after the Big Bang. *Nat. Astron.* **2024**, *8*, 657–672. [CrossRef]
100. Looser, T.J.; D'eugenio, F.; Maiolino, R.; Witstok, J.; Sandles, L.; Curtis-Lake, E.; Chevallard, J.; Tacchella, S.; Johnson, B.D.; Baker, W.M.; et al. A recently quenched galaxy 700 million years after the Big Bang. *Nature* **2024**, *629*, 53–57. [CrossRef] [PubMed]
101. Long, A.S.; Antwi-Danso, J.; Lambrides, E.L.; Lovell, C.C.; de la Vega, A.; Valentino, F.; Zavala, J.A.; Casey, C.M.; Wilkins, S.M.; Yung, L.Y.; et al. Efficient NIRCam Selection of Quiescent Galaxies at 3 < z < 6 in CEERS. *arXiv* **2023**, arXiv:2305.04662.
102. Haro, P.A.; Dickinson, M.; Finkelstein, S.L.; Fujimoto, S.; Fernández, V.; Kartaltepe, J.S.; Jung, I.; Cole, J.W.; Burgarella, D.; Chworowsky, K.; et al. Spectroscopic Confirmation of CEERS NIRCam-selected Galaxies at z $\sim$*eq* 8–10. *Astrophys. J. Lett.* **2023**, *951*, L22. [CrossRef]
103. Eilers, A.-C.; Simcoe, R.A.; Yue, M.; Mackenzie, R.; Matthee, J.; Ďurovčíková, D.; Kashino, D.; Bordoloi, R.; Lilly, S.J. EIGER. III. JWST/NIRCam Observations of the Ultraluminous High-redshift Quasar J0100+2802. *Astrophys. J.* **2023**, *950*, 68. [CrossRef]
104. Schneider, R.; Valiante, R.; Trinca, A.; Graziani, L.; Volonteri, M.; Maiolino, R. Are we surprised to find SMBHs with JWST at z > 9? Mon. *Not. R. Astron. Soc.* **2023**, *526*, 3250–3261. [CrossRef]
105. Chen, Y.; Mo, H.J.; Wang, K. Massive dark matter haloes at high redshift: Implications for observations in the JWST era. *Mon. Not. R. Astron. Soc.* **2023**, *526*, 2542–2559. [CrossRef]
106. Mauerhofer, V.; Dayal, P. The dust enrichment of early galaxies in the JWST and ALMA era. *Mon. Not. R. Astron. Soc.* **2023**, *526*, 2196–2209. [CrossRef]
107. Dirac, P.A.M. The Cosmological Constants. *Nature* **1937**, *139*, 323. [CrossRef]
108. Zwicky, F. On the redshift of spectral lines through interstellar space. *Proc. Natl. Acad. Sci. USA* **1929**, *15*, 773–779. [CrossRef]
109. Scolnic, D.; Brout, D.; Carr, A.; Riess, A.G.; Davis, T.M.; Dwomoh, A.; Jones, D.O.; Ali, N.; Charvu, P.; Chen, R.; et al. The Pantheon+ Analysis: The Full Data Set and Light-curve Release. *Astrophys. J.* **2022**, *938*, 113. [CrossRef]
110. Brout, D.; Scolnic, D.; Popovic, B.; Riess, A.G.; Carr, A.; Zuntz, J.; Kessler, R.; Davis, T.M.; Hinton, S.; Jones, D.; et al. The Pantheon+ Analysis: Cosmological Constraints. *Astrophys. J.* **2022**, *938*, 110. [CrossRef]
111. Gupta, R.P. Varying Coupling Constants and Their Interdependence. *Mod. Phys. Lett. A* **2022**, *37*, 2250155, arXiv: 2201.11667 (corrected version). [CrossRef]
112. Ryden, B.S. *Introduction to Cosmology*; Cambridge University Press: Cambridge, UK, 2017.
113. Baumann, D. *Cosmology*; Cambridge University Press: Cambridge, UK, 2022.
114. Longair, M.S. *Galaxy Formation*, 3rd ed.; Springer: Berlin/Heidelberg, Germany, 2023.
115. Laursen, P. Galaxy formation from a timescale perspective. In *Multiplicity of Time Scales in Complex Systems*; Springer: Berlin/Heidelberg, Germany, 2023.
116. Cao, S.; Ryan, J.; Ratra, B. Using Pantheon and DES supernova, baryon acoustic oscillation, and Hubble parameter data to constrain the Hubble constant, dark energy dynamics, and spatial curvature. *Mon. Not. R. Astron. Soc.* **2021**, *504*, 300–310. [CrossRef]
117. Cao, S.; Ratra, B. H0 = 69.8 $\pm$ 1.3 km s^{-1} Mpc^{-1}, Ωm0 = 0.288 $\pm$ 0.017, and other constraints from lower-redshift, non-CMB, expansion-rate data. *Phys. Rev. D* **2023**, *107*, 103521. [CrossRef]
118. Peng, P. The Pantheon Sample analysis of cosmological constraints under new models. *arXiv* **2023**, arXiv:2303.10095.
119. Eappen, R.; Kroupa, P. The formation of compact massive relic galaxies in MOND. *Mon. Not. R. Astron. Soc.* **2024**, *528*, 4264–4271. [CrossRef]

120. Garcia-Bellido, J.; Hawkins, M. Reanalysis of the MACHO constraints on PBH in the light of Gaia DR3 data. *arXiv* **2024**, arXiv:2402.00212.
121. Lee, S. Constraint on the minimally extended varying speed of light using time dilations in Type Ia supernovae. *Mon. Not. R. Astron. Soc.* **2023**, *524*, 4019–4023. [CrossRef]
122. Lewis, G.F.; Brewer, B.J. Detection of the Cosmological Time Dilation of High-Redshift Quasars. *Nat. Astron.* **2023**, *7*, 1265–1269. [CrossRef]
123. Hawkins, M.R.S. On time dilation in quasar light curves. *Mon. Not. R. Astron. Soc.* **2010**, *405*, 1940–1946. [CrossRef]
124. Blondin, S.; Davis, T.M.; Krisciunas, K.; Schmidt, B.P.; Sollerman, J.; Wood-Vasey, W.M.; Becker, A.C.; Challis, P.; Clocchiatti, A.; Damke, G.; et al. Time Dilation in Type Ia Supernova Spectra at High Redshift. *Astrophys. J.* **2008**, *682*, 724–736. [CrossRef]
125. Lesgourgues, J. The Cosmic Linear Anisotropy Solving System (CLASS) I: Overview. *arXiv* **2011**, arXiv:1104.2932.
126. Lewis, A.; Challinor, A.; Lasenby, A. Efficient Computation of Cosmic Microwave Background Anisotropies in Closed Friedmann-Robertson-Walker Models. *Astrophys. J.* **2000**, *538*, 473–476. [CrossRef]
127. Wang, C.; Bolejko, K.; Lewis, G.F. The Instantaneous Redshift Difference of Gravitationally Lensed Images: Theory and Observational Prospects. *Astrophys. J.* **2022**, *940*, 16. [CrossRef]
128. Wang, C.; Bolejko, K.; Lewis, G.F. The Redshift Difference in Gravitational Lensed Systems. *Mon. Not. R. Astron. Soc.* **2023**, *525*, 3006–3015. [CrossRef]
129. Cao, S.; Qi, J.; Biesiada, M.; Zheng, X.; Xu, T.; Zhu, Z.-H. Testing the Speed of Light over Cosmological Distances: The Combination of Strongly Lensed and Unlensed Type Ia Supernovae. *Astrophys. J.* **2018**, *867*, 50. [CrossRef]
130. Cao, S.; Qi, J.; Biesiada, M.; Liu, T.; Zhu, Z.-H. Precise Measurements of the Speed of Light with High-redshift Quasars: Ultra-compact Radio Structure and Strong Gravitational Lensing. *Astrophys. J.* **2020**, *888*, L25. [CrossRef]
131. Gupta, R.P. Testing the Speed of Light Variation with Strong Gravitational Lensing of SNe 1a. *Res. Notes AAS* **2021**, *5*, 176. [CrossRef]